



Iron oxide nanoparticles supported on diamond nanoparticles as efficient and stable catalyst for the visible light assisted Fenton reaction

Juan C. Espinosa^{a,b}, Cristina Catalá^{a,b}, Sergio Navalón^{a,*}, Belén Ferrer^{a,b}, Mercedes Álvaro^a, Hermenegildo García^{a,b,*}

^a Departamento de Química and Instituto Universitario de Tecnología Química CSIC-UPV, Universitat Politècnica de València, Consejo Superior de Investigaciones Científicas, Av. de los Naranjos s/n, 46022 Valencia, Spain

^b Center of Excellence for Advanced Materials Research, King Abdulaziz University, Jeddah, Saudi Arabia



ARTICLE INFO

Keywords:

Heterogeneous catalysis
PhotoFenton reaction
Waste water treatment
Iron oxide nanoparticles
Diamond nanoparticles

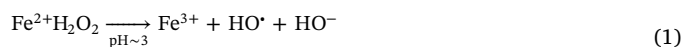
ABSTRACT

Iron oxide nanoparticles (Fe_{ox} NPs) have been supported on the hydroxylated surface of modified diamond nanoparticles (D3). Characterization data show that, once formed, Fe NPs are spontaneously oxidized under ambient conditions, exhibiting a good dispersion of small oxidized Fe_{ox} NPs ($2.2 \pm 0.5 \text{ nm}$) on D3. It has been observed that the activity of $\text{Fe}_{\text{ox}}/\text{D}3$ as heterogeneous Fenton catalyst for phenol degradation by H_2O_2 can be assisted by visible light irradiation. $\text{Fe}_{\text{ox}}/\text{D}3$ exhibits a superior activity compared with analogous catalysts based on activated carbon, graphite or the benchmark $\text{Fe}_{\text{ox}}/\text{TiO}_2$ photocatalyst. $\text{Fe}_{\text{ox}}/\text{D}3$ exhibits comparable activity to $\text{Ag}/\text{D}3$ that is one of the most active catalysts ever reported for this reaction. In addition, $\text{Fe}_{\text{ox}}/\text{D}3$ presents higher stability and recyclability than analogous $\text{Cu}/\text{D}3$. A minimum accumulated turnover number of 38,000 can be achieved using $\text{Fe}_{\text{ox}}/\text{D}3$ as photocatalyst. The heterogeneous photoFenton process using phenol as model pollutant and $\text{Fe}_{\text{ox}}/\text{D}3$ as catalyst under visible light irradiation can be implemented prior to an aerobic biological treatment resulting in a biodegradable effluent which lacks ecotoxicity, as determined by measurement of the biological oxygen demand. Transient absorption spectroscopy provides evidence in support of the formation upon irradiation of $\text{Fe}_{\text{ox}}/\text{D}3$ of photogenerated charge separation state attributed to electrons and holes. Electron paramagnetic resonance and selective quenching experiments indicate that hydroxyl radicals are the main reactive oxygen species generated in the photo-assisted Fenton reaction promoted by $\text{Fe}_{\text{ox}}/\text{D}3$.

1. Introduction

Advanced oxidation processes (AOPs) are among the common technologies for pollutant degradation in water [1–7]. The main objective of AOPs is the generation of reactive oxygen species (ROS) able to degrade or even mineralize organic pollutants [2,3]. Generally, AOPs are employed for the degradation of recalcitrant, toxic and non-biodegradable compounds that cannot be removed by conventional biological treatments [3,8]. Among the different AOPs, the Fenton reaction and its light-assisted version are some of the preferred processes for the generation of highly aggressive hydroxyl radicals (Eqs. (1) and (2)). The main drawbacks, however, of this process include [5,9,10]: i) requirement of acidic water pH values in which the photoactive Fe(OH)^{2+} aqueous complex is the predominant Fe species, ii) the use of artificial UV-vis light; iii) the need to remove the iron species by precipitation with subsequent sludge formation; iv) the high H_2O_2 excess required due to the occurrence of undesirable side reactions leading to spurious

decomposition of hydrogen peroxide to H_2O and O_2 . These problems associated with homogeneous processes can be partially solved by heterogeneous catalysis [3,11–14]. The most commonly employed solids as heterogeneous Fenton catalysts are aluminosilicates [11], carbonaceous materials [14] and supported or unsupported metal or metal oxide nanoparticles (NPs) [13].



In the field of metal NPs, Garcia et al. have reported that metal NPs exhibiting plasmonic absorption bands in the visible region such as Au [8], Ag [15] and Cu [16] supported on surface modified diamond (D) NPs are among the most effective catalysts to promote the heterogeneous (photo)Fenton reaction under visible and solar light irradiation even at quasi-neutral pH values. It is important to note that analogous

* Corresponding authors at: Departamento de Química and Instituto Universitario de Tecnología Química CSIC-UPV, Universitat Politècnica de València, Consejo Superior de Investigaciones Científicas, Av. de los Naranjos s/n, 46022, Valencia, Spain.

E-mail addresses: sernaol@doctor.upv.es (S. Navalón), hgarcia@qim.upv.es (H. García).

(photo)catalysts using other carbonaceous supports such as graphite (G), activated carbon (AC) or multiwall-carbon nanotubes (MWCNTs) resulted in lower activity and/or efficiency for this process. Besides the noble metals supported on D, it is of interest for the sake of sustainability to develop other alternatives based on cost-effective catalyst employing more abundant and affordable metals. One of the main problems associated with the use of supported non-noble metals as catalysts for the heterogeneous (photo)Fenton reactions is their poor stability under strong oxidation conditions and also the occurrence in a large extent of metal leaching [13]. Thus, developing an appropriate support to strongly anchor and immobilize non-noble metal NPs without decreasing their effectiveness as (photo)catalyst at neutral pH values remains a challenge in this area [13,14]. Recently, Cu NPs supported on D have been reported as an active catalyst for the heterogeneous (photo)Fenton reaction under visible light irradiation even at quasi-neutral pH values [16]. However, Cu supported on D becomes deactivated upon reuse due to the oxidation of the active reduced copper species to inactive Cu(II) and, therefore, subsequent chemical reduction of the Cu catalyst to regenerate the catalyst before reuse is needed.

In the present work, it will be reported that Fe_{ox} NPs supported on the hydroxylated surface of modified D NPs shows high activity and efficiency in terms of H₂O₂ consumption for the heterogeneous (photo) Fenton reaction using both artificial and natural visible light irradiation at quasi-neutral pH values. Furthermore, the solid catalyst can be easily recovered by filtration, washed with basic water and, then, reused without the need of any additional pretreatment. Importantly, iron leaching from the solid catalyst to the solution can be almost suppressed working at pH values above pH 6. The heterogeneous process can be coupled with an aerobic biological treatment for the remediation of a waste water model solution containing phenol as probe. Transient absorption spectroscopy indicates that supported Fe_{ox} NPs on surface hydroxylated D NPs (D3) behave as a semiconductor undergoing charge separation under visible light irradiation. Experimental evidence indicates that the main reactive oxygen species (ROS) generated by the D supported iron oxide is hydroxyl radical as it occurs in the conventional homogeneous Fenton reaction.

2. Experimental section

2.1. Materials

Diamond NPs (D; ref: 636444, ≥97%, ~80 €/g), graphite (G, < 20 mm, ref. 282863), activated carbon (AC; Norit SX Ultra, ref. 53663), iron(II) sulfate heptahydrate (> 99%), dimethylsulfoxide (DMSO, > 99.5%), *p*-benzoquinone (> 98%) and 5,5-dimethyl-1-pyrrolidine N-oxide (DMPO) were supplied by Sigma-Aldrich. TiO₂ (P-25) was supplied by Evonik. Reagents or solvents were of analytical or HPLC grade.

2.2. Catalyst preparation

The catalysts were prepared by deposition of metal NPs (Fe, Cu or Ag) on commercial carbonaceous materials with or without surface modification by chemical or thermal treatments according previously reported procedures [17]. The chemical functionalization of the carbonaceous materials (D, AC and G) consists in a homogeneous Fenton treatment leading to the supports labelled as D2, G2 and AC2 [15]. These D2, G2 and AC2 samples were subsequently submitted to H₂ annealing at 500 °C. Metal deposition on the different carbonaceous materials (D1-3, AC1-3 and G1-3) was carried out employing the polyol method following reported procedures [18]. Briefly, 200 mg of carbonaceous material was suspended in ethylene glycol, then, the metal salt precursor dissolved in water was added to the suspension and, finally, the system heated at 85 °C for 5 h. The materials were thoroughly washed using acetone and water and, then, dried under vacuum.

Analogously iron NPs were deposited on commercial benchmark photocatalyst TiO₂ (P-25).

Unsupported iron NPs were prepared by chemical reduction of an iron(II) salt solution (25 mL) by addition of 10-fold excess NaBH₄ at room temperature [16].

2.3. Catalyst characterization

Transmission electron microscopy (TEM) images in dark (DF-STEM) or bright field were recorded on a JEOL JEM2100F instrument operating at 200 kW. Metal particle size distribution was estimated by counting more than 300 particles from the sample. Powder X-ray diffractograms (PXRD) were recorded using a Philips XPert diffractometer equipped with a graphite monochromator (40 kV and 45 mA) employing Ni filtered CuK α radiation. Inductively coupled plasma-atomic emission spectroscopy (ICP-AES) was employed to confirm the catalyst metal loading (0.2 or 1 wt%) and the possible iron leaching from previously filtered reaction aliquots (0.2 μm Nylon) at the end of the reaction.

2.4. Photocatalytic experiments

Photocatalytic experiments were carried out under natural (June–July 2016, Technical University of Valencia, Valencia, Spain; irradiation intensity $971 \pm 32 \text{ mW cm}^{-2}$ and $28 \pm 1.9^\circ\text{C}$) or artificial (Solar simulator ORIEL Sol 1A) Sunlight irradiation. The experiments were performed at least three times. A round-bottom flask (500 mL) containing a phenol solution (25 mL; 100 mg L⁻¹, 1.06 mM) and the corresponding amount of catalyst (i.e. 0.0072 mM of the supported metal NP) was sonicated for 20 min. Then, the initial pH value of the aqueous mixture was adjusted to the required value using HNO₃ (0.1 M) or NaOH (0.1 M) aqueous solutions. Subsequently, the required amount of H₂O₂ was added to the reaction mixture and the system irradiated using natural or simulated sunlight. In the case of natural Sunlight irradiations the samples were equilibrated at the ambient temperature before addition of H₂O₂. A calibrated photodiode connected to a voltmeter was employed to measure the solar irradiation intensity. In order to minimize the possible metal leaching from the solid catalyst to the solution, the pH of the reaction was maintained above a pH specific value. For example, for experiments carried out at pH 4, the pH value was not allowed to be below this value. A minimum pH value of 5.5 was set for experiments carried out at pH 6 or 7. For experiments performed at basic conditions a minimum pH value of the reaction mixture of 7 was set.

To study the reusability of the catalyst, the solid material was recovered by filtration through a Nylon membrane filter (0.2 μm pore size), washed with a basic aqueous solution (pH 10) to remove possible adsorbed organic compounds and, then, with Milli-Q water to neutralize the basic pH value. Then, a subsequent photocatalytic reaction was carried out. This process was repeated two more times.

A productivity test was also carried out in a round-bottom flask (25 mL) using a high excess of phenol (25 g L⁻¹) and H₂O₂ (100 g L⁻¹) respect to the catalyst (80 mg L⁻¹). Three reuse experiments were also carried out under high substrate-catalyst ratio using the above commented procedure for catalyst recovery and washings.

2.5. Biodegradability experiments

The ratio of biological oxygen demand at 5 days (BOD₅) to the chemical oxygen demand (COD) was used as the biodegradability index. At the end of each photocatalytic experiment, when the H₂O₂ concentration was zero, the sample was filtered under vacuum through a 0.2 μm Nylon membrane. For BOD₅ measurement, the samples were transferred to a commercially available 300 mL BOD-bottle (Lovibond; 300 mL), aerated at 20 °C for 1 h under magnetic stirring and buffered at pH 7 (K₂HPO₄/KH₂PO₄, 0.01 M). Afterwards, activated sludges from

the sediment of a waste water treatment plant were added (1 g/L) and the bottle closed using a BOD-Sensor (Lovibond OxiDirect) cap before incubation at 20 °C under continuous stirring for 5 days. At this time, the BOD-Sensor displays the BOD₅ value (mg/L of O₂) (Standard Methods, 5210) [19]. In addition, a filtered reaction aliquot sample (0.2 µm Nylon filter) was analysed by HPLC-RF-UV (see below). COD was determined using the dichromate method (Standard Methods, 5220D) [19]. Accordingly to the Standard Methods procedure, BOD₅ blank control experiments were performed by using a solution of glucose (150 mg L⁻¹) and glutamic acid (150 mg L⁻¹), resulting in a BOD₅ value of ~198 mg L⁻¹ [19].

2.6. Reaction analyses

Filtered reaction aliquots (0.2 µm Nylon membrane) were analyzed by reverse phase-chromatography using a Kromasil-C18 column as stationary phase, eluting under isocratic conditions (69/30/1 v%, H₂O/CH₃CN/CH₃COOH) and using a photodiode array detector. The samples of the productivity test were 250-fold diluted in Milli-Q water before analysis. As previously reported, H₂O₂ concentration was determined using a colorimetric method that employs as solution of K₂(TiO)(C₂O₄)₂ in H₂SO₄/HNO₃ as indicator monitoring at 420 nm and using a calibration plot [20]. Before measurements the sample aliquots were diluted 10-fold, except in the case of productivity tests were the samples were diluted by a factor of 5000 times.

2.7. EPR measurements

EPR spectra using DMPO as spin trap were carried out as follows: catalyst (100 mg L⁻¹), DMPO (1000 mg L⁻¹), H₂O₂ to DMPO molar ratio 1, pH 4, artificial solar light irradiation, reaction time 5 min. Filtered (0.2 µm) and nitrogen-purged aliquots were measured on a Bruker EMX spectrometer using the following typical settings: frequency 9.803 GHz, sweep width 3489.9 G, time constant 40.95 ms, modulation frequency 100 kHz, modulation width 1 G, microwave power 19.92 mW.

2.8. Selective radical scavenger experiments

DMSO or *p*-benzoquinone were used as selective hydroxyl or hydroperoxyl radical scavengers, respectively [13]. The quenching experiments were carried out under the following reaction conditions: catalyst (100 mg L⁻¹), phenol (100 mg L⁻¹), H₂O₂ (200 mg L⁻¹), radical scavenger to H₂O₂ molar ratio 10, pH 4, artificial solar light irradiation.

2.9. Total organic carbon (TOC) measurements

TOC of phenol samples were analyzed using a High TOC Elementar II analyzer.

3. Results and discussion

3.1. Catalyst preparation and characterization

This section presents the characterization data of the catalysts prepared in the present work. In the first step, the surface of commercial carbonaceous materials (D NPs, AC and graphite) were modified by submitting the solids to a homogeneous Fenton treatment followed or not by a hydrogen annealing process at high temperature, as previously reported for the preparation of different metals (Au, Ag and Cu) supported on D [15,16]. The aim of the chemical treatment is to remove impurities and introduce oxygen functional groups on the surface of the carbonaceous supports that would make the surface of the material more adequate to support in a second step small metal NPs compared to the dimensions of these metal NPs absorbed directly on commercial

Table 1

List of catalysts (0.2 wt% metal loading) employed in the present work indicating metal average particle size and initial reaction rate and final conversion for phenol degradation.

Entry	Catalysts	Metal particle size and standard deviation (nm) ^a	Initial reaction rate (mM h ⁻¹) ^e	Phenol conversion at 3.2 h (%)	Turnover frequency (h ⁻¹)
1	Fe _{ox} /AC1	19.2 ± 3.1	0.07	35	16.2
2	Fe _{ox} /AC2	14.1 ± 2.4	0.11	46	21.3
3	Fe _{ox} /AC3	12.2 ± 2.1	0.11	72	33.4
4	Fe _{ox} /G1	18.5 ± 2.5	0.11	50	23.2
5	Fe _{ox} /G2	15.2 ± 1.9	0.21	74	34.3
6	Fe _{ox} /G3	13.1 ± 1.5	0.21	80	37.1
7	Fe _{ox} /D1	5.2 ± 1.7	0.13	63	29.2
8	Fe _{ox} /D2	4.1 ± 1.1	0.26	75	34.8
9	Fe _{ox} /D3	2.2 ± 0.5	0.62	100	46.4
10	Fe _{ox} /D3 ^b	2.4 ± 0.4	0.31	90	41.7
11	Cu/D3 ^c	3.7 ± 2.7	0.77	100	46.4
12	Ag/D3 ^c	3.2 ± 2.7	0.77	100	46.4
13	Fe _{ox} /TiO ₂	4.9 ± 2.7	1.17	92	42.7
14	TiO ₂ ^d	—	0.38	49	—

^a Average metal particle size estimated from the DF-STEM images presented in the supplementary material (Figs. S1–S4).

^b 1 wt% metal loading catalyst.

^c These catalysts have been previously reported in Refs. [15,16] and they correspond to the same batch employed in the present work.

^d No metal loading.

^e Reaction conditions: catalyst (100 mg L⁻¹), phenol (100 mg L⁻¹), H₂O₂ (200 mg L⁻¹), pH 4, simulated solar light irradiation.

supports. Subsequent hydrogen annealing of the carbonaceous materials at 500 °C results in the formation of a more homogeneous hydroxylated carbon surface. The presence of hydroxyl groups on the various carbon materials has been found beneficial to achieve and maintain metal NPs of small particle size supported on the carbonaceous material respect to the Fenton-treated materials [15,16]. In accordance with these precedents, the smallest average particle size distribution and narrower standard deviation of supported iron NPs in the different carbonaceous supports under study (AC, G and D) were obtained also in the present case when using a Fenton-treatment followed by annealing under hydrogen (Table 1, entries 3, 6 and 9). In the case of the Fenton-treated carbonaceous supports, the particle size distribution and standard deviation is also smaller respect to the commercial samples (Table 1, entries 2, 5 and 8 vs 1, 4 and 7). For the most appropriate material to support the smallest Fe_{ox} NPs, D3, it was observed that an increase of the iron loading from 0.2 to 1 wt% has only a minor influence on the average particle size distribution (Table 1, entries 9 and 10).

To put into context the catalytic activity of these materials based on Fe_{ox} NPs supported on carbonaceous materials, analogous catalysts based on Ag or Cu NPs supported on D3 as well as Fe_{ox}/TiO₂ as benchmark photocatalyst were also prepared (Table 1, entries 11–13).

The presence of iron oxide NPs was confirmed by means of an EDX detector coupled with the TEM instrument employed for particle size counting (Figs. S4–S7). PXRD measurements of the Fe_{ox}(0.2 wt%)/D3 catalyst with the smallest particle size distribution did not show the presence of any of the characteristic iron or iron oxide diffraction peaks (Fig. S8). This fact may be a reflection of the small iron NPs and/or good dispersion of the iron NPs on the support as evidenced by TEM measurements (Fig. 1) [15,16]. Diffuse reflectance measurements reveal the presence of absorption bands characteristic of iron oxides such as Fe₂O₃ (Fig. S9) [21]. Formation of iron oxide occurs spontaneously upon ambient exposure due to the presence of O₂ and H₂O [22]. Control experiments showed that unsupported zero valence iron NPs, prepared by chemical reduction of Fe(III) by NaBH₄ [16], are oxidized under ambient conditions as revealed by the changes in the UV-vis spectrum and the usual appearance of the solution becoming brown in a few

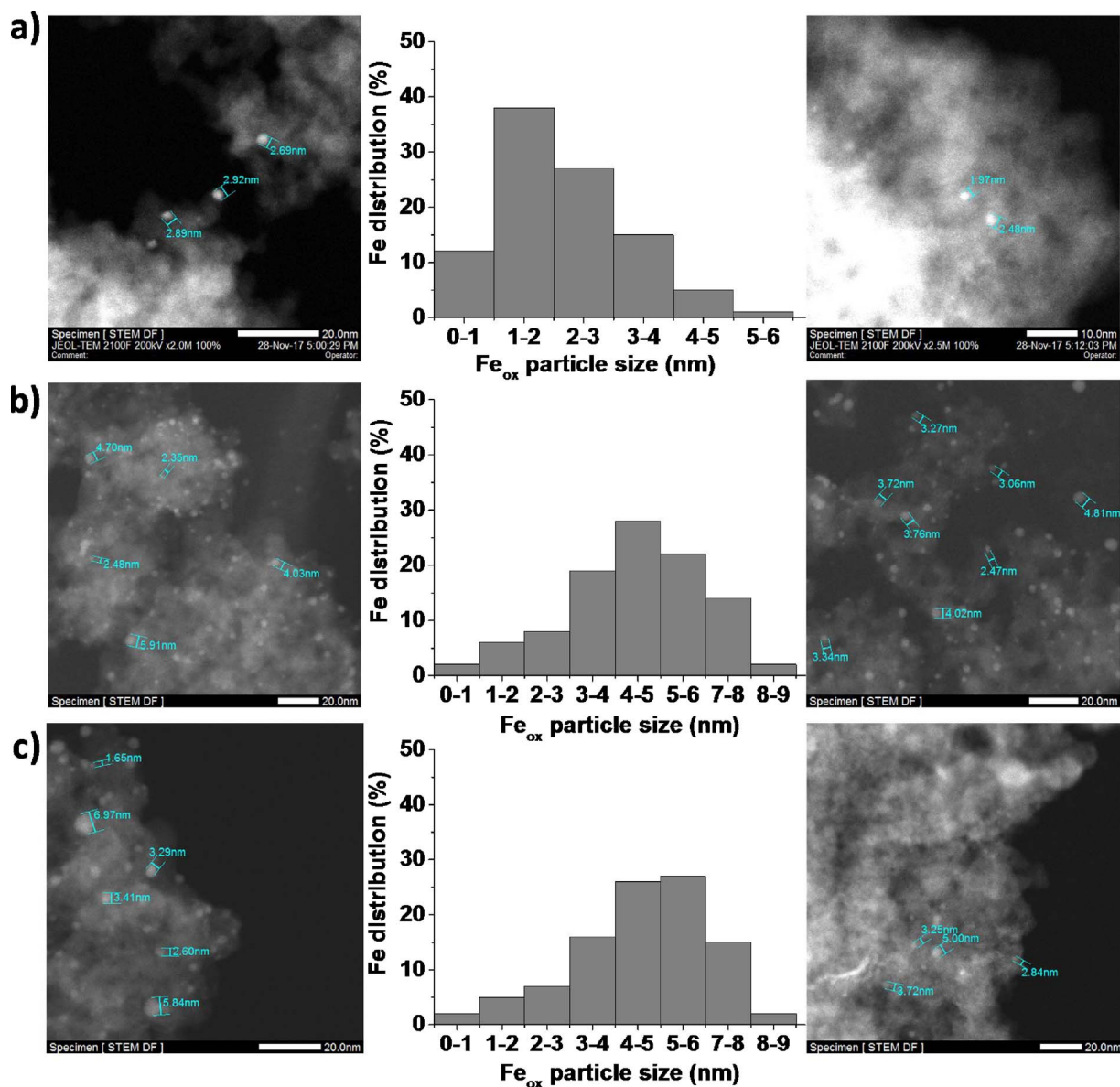


Fig. 1. DF-STEM images and histograms of particle size distribution of fresh (a), four times used (b) and eight times used (c) $\text{Fe}_{\text{ox}}(0.2 \text{ wt}\%)$ /D3 catalyst.

minutes due to the oxidation of Fe NPs to iron oxide particles under ambient conditions (see photographs in Fig. S10). The presence of iron oxides supported on D3 was also established by FT-IR spectroscopy where the characteristic Fe–O vibration bands of iron oxides can be observed in the region between 700 and 400 cm^{-1} for the $\text{Fe}_{\text{ox}}(0.2 \text{ and } 1.0 \text{ wt}\%)$ /D3 samples as well as for commercial Fe_2O_3 and Fe_3O_4 standards (Fig. S11) [23]. EPR analysis of $\text{Fe}(0.2 \text{ wt}\%)$ /D3 sample confirms the presence of Fe(III) in the $\text{Fe}(0.2 \text{ wt}\%)$ /D3 sample (Fig. S12) [24]. It should be noted that Fe(II) species are EPR-silent. XPS of $\text{Fe}(0.2 \text{ wt}\%)$ /D3 and $\text{Fe}(1.0 \text{ wt}\%)$ /D3 confirms that most of the surface of the iron NPs is composed by Fe(III) (Fig. S13) [25]. All together, the available characterization data points out that the Fe_{ox} NPs supported on D3 are at least partially oxidized.

3.2. Photocatalytic activity

The catalytic activity of the prepared materials has been tested for phenol degradation and H_2O_2 decomposition under simulated solar light irradiation. Phenol was selected as model pollutant due to its high toxicity and lack of biodegradability by conventional biological treatments [8,26]. Preliminary control experiments were carried out by: i)

irradiating with simulated sunlight phenol and H_2O_2 in the absence of catalyst; ii) simulated sunlight irradiation of phenol in the presence of $\text{Fe}_{\text{ox}}/\text{D3}$ catalysts in the absence of H_2O_2 ; iii) irradiation with simulated sunlight phenol and H_2O_2 in the presence of the D supports (no Fe_{ox}), iv) performing the reaction of phenol and H_2O_2 in the presence of $\text{Fe}_{\text{ox}}/\text{D3}$ in the dark, whereby a very minor degree of phenol disappearance of H_2O_2 consumption was observed. Figs. S14 and S15 in the supporting information show the results of all these blank controls that confirm that the combination of iron oxide, simulated sunlight and H_2O_2 is necessary to achieve high percentages of phenol degradation.

Then, the photocatalytic activity of the Fe_{ox} NPs supported on D NPs modified by chemical treatments was studied for phenol degradation and H_2O_2 decomposition. $\text{Fe}_{\text{ox}}(0.2 \text{ wt}\%)$ /D3 exhibits higher photocatalytic activity than $\text{Fe}_{\text{ox}}/\text{D2}$ and $\text{Fe}_{\text{ox}}/\text{D1}$ (Table 1 and Fig. S16). This fact can be attributed to the smallest average particle size distribution and a more uniform size distribution of supported Fe_{ox} NPs when using D3 as support (Table 1 and Fig. S16). Phenol adsorption on $\text{Fe}_{\text{ox}}/\text{D3}$ was estimated to be less than 3 wt% and, therefore, the influence of adsorption on the measurements of phenol degradation should be very little. The activity of $\text{Fe}_{\text{ox}}/\text{D3}$ is also higher than analogous photocatalysts based on $\text{Fe}_{\text{ox}}/\text{AC3}$ or $\text{Fe}_{\text{ox}}/\text{G3}$ (Fig. 2). Activity data show that

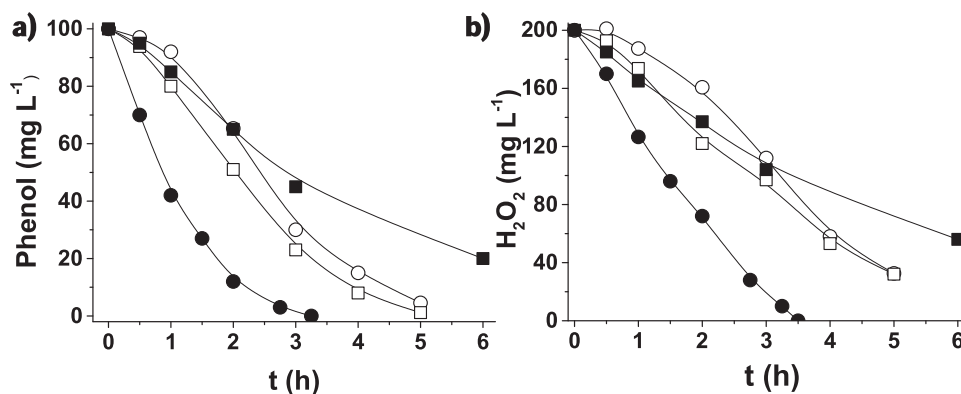


Fig. 2. Temporal profile of phenol degradation (a) and H₂O₂ decomposition (b) using Fe_{ox}(0.2 wt%)/D3 (●), G3 (□) and AC3 (○) under simulated sunlight irradiation. A control experiment using Fe_{ox}(0.2 wt %)/D3 under dark conditions is also shown (■). Reaction conditions: Catalyst (200 mg L⁻¹, 0.0072 mM), phenol (100 mg L⁻¹, 1.06 mM), H₂O₂ (200 mg L⁻¹, 5.88 mM), pH 4, sunlight intensity (100 mW cm⁻²), 20 °C.

regardless the carbonaceous support (D, AC or G), surface modification by a Fenton treatment using a soluble Fe^{II} salt, followed by hydrogen annealing at high temperature is an adequate surface treatment to prepare samples with small Fe_{ox} NP size and enhanced catalytic activity (Table 1 and Fig. S1). The activity of the Fe_{ox} NPs supported on Fenton-treated carbon materials (AC2, G2 and D3) is higher than that achieved using commercial carbon samples (AC1, G1 and D1) as supports. This data is in agreement with previous reports highlighting the benefits of having hydroxyl groups on the surface of the supports to stabilize small metal NPs. Importantly, the catalytic activity of the most active photocatalyst (Fe_{ox}/D3) is almost double than that of unsupported Fe_{ox} NPs, a fact that was attributed to the observed agglomeration of unsupported Fe_{ox} NPs after preparation (Fig. S10) [27]. The Fe_{ox}/D3 sample with 0.2 wt% exhibited higher activity at the same iron content than a similar sample containing 1 wt% (5-fold less weight), a fact that can be understood considering the higher Fe_{ox} dispersion and the somewhat lower average particle size distribution (Table 1 and Fig. S17). It is a general observation in heterogeneous catalysis that an increase in the loading of the metal results in somewhat lower turnover numbers due to the general trend in particle size increase and decrease in metal dispersion [16,28].

Importantly, the efficiency of Fe_{ox}/D3 is higher than that of the benchmark photocatalyst Fe_{ox}/TiO₂ that rapidly decomposes H₂O₂, but without achieving full degradation of phenol (Table 1 and Fig. 3). As previously reported TiO₂ decomposes H₂O₂ to H₂O and O₂ without generating a high density of reactive oxygen species able to degrade phenol [15]. This observation was confirmed by using solely TiO₂ and observing that H₂O₂ decomposes completely, but without promoting the complete degradation of phenol (Fig. 3). In addition, the concentration of phenol and its reaction intermediates is zero when using Fe_{ox}/D3, while the sum of the concentration of all these compounds in the case of using Fe_{ox}/TiO₂ or TiO₂ still is 50 and 89 mg L⁻¹, respectively (Fig. S18).

The photocatalytic activity of the most active catalyst prepared in

the present work Fe_{ox}/D3 was also compared with that of analogous D3 supported catalysts based on Ag and Cu NPs (Table 1 and Fig. S19). Ag/D3 shows higher photocatalytic activity compared to Fe_{ox}/D3 and Cu/D3. This fact is not unexpected since Ag/D3 is one of the most active photocatalysts ever reported for the heterogeneous (photo)Fenton reaction under visible light irradiation [15]. Nevertheless, it would be advantageous to replace silver by other cost-effective transition metal, while still maintaining catalytic activity high. In this sense, Cu/D3 has been reported as an alternative to the use of Ag/D3. However, Cu/D3 suffers from severe deactivation during the reaction a fact that was attributed to the partial oxidation of Cu NPs to catalytically inactive Cu²⁺ species [16]. In fact, the activity of the used Cu/D3 can be recovered in some extent by reducing again the partially oxidized used Cu/D3 in hot ethylene glycol. As it will be commented later, Fe_{ox}/D3 can be reused several times without the need of additional reductive pre-treatments like in the case of Cu/D3.

One of the most important current limitations in both homogeneous and heterogeneous catalysts is how to promote the (photo)Fenton reaction at neutral pH value without the need of an extremely large H₂O₂ excess [1,9]. Typically the (photo)Fenton process is limited at acidic pH values. Fig. 4 shows that Fe_{ox}/D3 can act as an efficient photocatalysts at initial pH values between 4 and 6 under simulated Sunlight irradiation at 20 °C. Interestingly, natural Sunlight irradiations at ambient conditions (971 mW/cm², 28 °C) can expand the initial pH values of the reaction using a 5-fold excess of H₂O₂ up to pH 6. However, observation in the temporal profiles of an induction period indicates that the reaction becomes accelerated as it proceeds and the pH value decreases from the initial value. Similar results were observed when using the catalyst based on the noble metal Ag NPs supported on D3 [15].

The influence of the H₂O₂ concentration on the photocatalytic activity for phenol degradation using Fe_{ox}/D3 was also evaluated. H₂O₂ is a relatively costly commodity and, therefore, its optimization is needed to keep low the operational costs of the Fenton process [13,14]. Interestingly, the heterogeneous photo-Fenton reaction using Fe_{ox}/D3 as

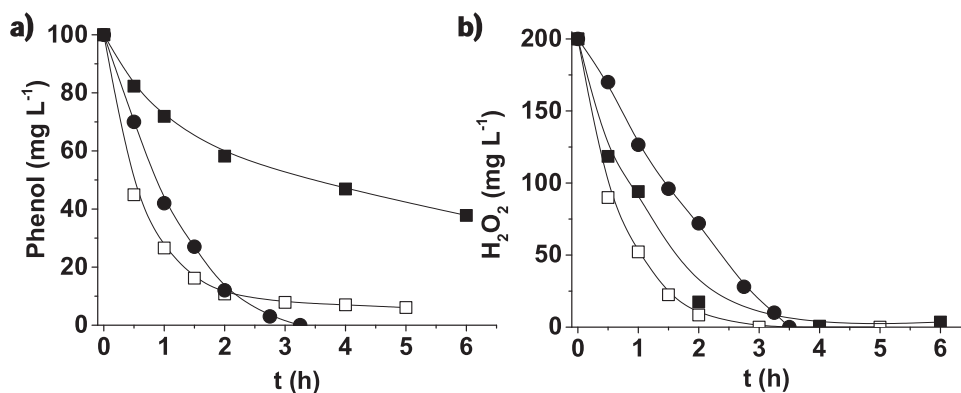


Fig. 3. Temporal profiles of phenol degradation (a) and H₂O₂ decomposition (b) using Fe_{ox}(0.2 wt%)/D3 (●), Fe_{ox}/TiO₂ (□) or TiO₂ (■) as heterogeneous (photo)Fenton catalysts under sunlight irradiation. Reaction conditions: Catalyst (200 mg L⁻¹, 0.0072 mM), phenol (100 mg L⁻¹, 1.06 mM), H₂O₂ (200 mg L⁻¹, 5.88 mM), pH 4, sunlight intensity (100 mW cm⁻²), 20 °C.

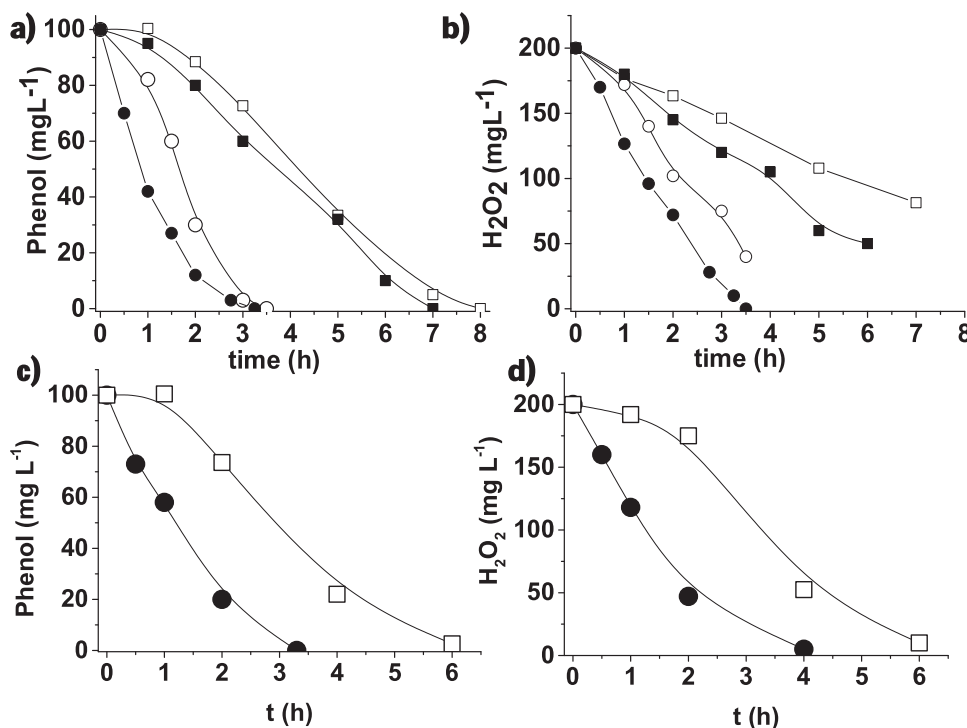


Fig. 4. Temporal profiles of phenol degradation (a, c) and H_2O_2 decomposition (b, d) using Fe_{ox} (0.2 wt %)/D3 at initial pH 4 (●), pH 4.5 (○), pH 5 (■) and pH 6 (□) under simulated (a, b) and natural Sunlight irradiation (c, d; 28 °C). Reaction conditions: 100 mg/L phenol, 200 mg/L H_2O_2 , suitable pH, 5 mg Fe_{ox} /D3 catalyst (0.2 wt%), 20 °C.

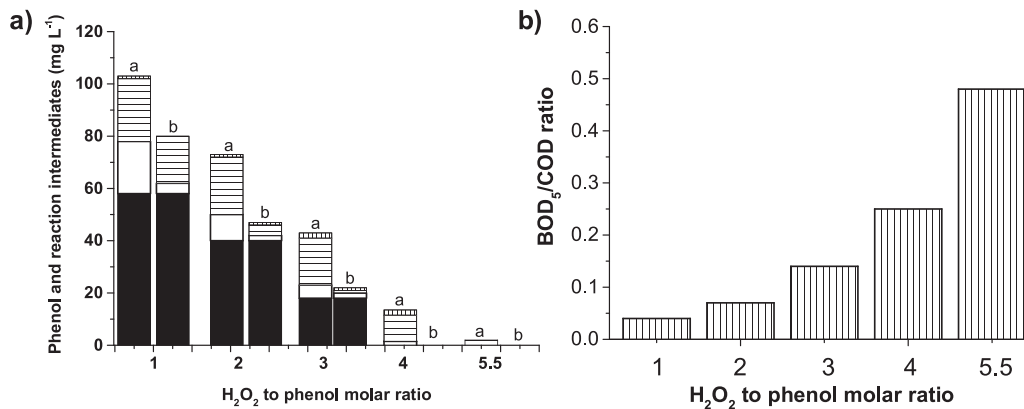


Fig. 5. Influence of H_2O_2 to phenol molar ratio on the final concentration of phenol and reaction intermediates (plot a) and on the biodegradability of the resulting effluent (BOD_5/COD , plot b). Legend: a) Phenol (black bar), hydroquinone (white bar), catechol (horizontal lines) and *p*-benzoquinone (vertical lines). Initial BOD_5 and COD values of the phenol solution (100 mg/L) are 0 and 105 mg/L, respectively; the concentration of phenol and its reaction intermediates refers to the point when H_2O_2 is completely decomposed.

catalyst can be combined with a biological aerobic treatment to obtain a biodegradable effluent free of ecotoxicity using a minimal amount of H_2O_2 . Fig. 5 shows that phenol degradation can be achieved under simulated Sunlight conditions with a H_2O_2 to phenol molar ratio as low as 4, although at this ratio ecotoxicity is still too high due to the presence of byproducts (vide infra). The biodegradability of water is defined the ratio between BOD_5 and COD [8]. A water is biodegradable when its BOD_5 to COD ratio is higher than 0.4. Phenol and several of its byproducts are not biodegradable under conventional biological aerobic treatments and they are toxic compounds [8]. In the case of phenol the term ecotoxicity is related with the absence of its degradation products, such as catechol, hydroquinone and *p*-benzoquinone that are even more toxic than phenol itself [8]. In this work a minimal H_2O_2 to phenol molar ratio of 5.5 is enough to obtain a non-ecotoxic (Fig. 5a) and biodegradable effluent ($\text{BOD}_5/\text{COD} > 0.4$, Fig. 5b). This result compares favorably with other Fenton catalysts based on transition metals that typically employ large excesses of H_2O_2 , not uncommonly over 1000 to achieve low ecotoxicity [13,14]. It is worth commenting that the theoretical H_2O_2 to phenol molar ratio needed for complete phenol mineralization exclusively by H_2O_2 is 14. However, in the present case the reactions were carried out under aerobic conditions and atmospheric oxygen should be contributing to degradation, decreasing

H_2O_2 requirements. In our case using a H_2O_2 to phenol molar ratio of 5.5 working at pH 4 under simulated Sunlight conditions a TOC reduction of 75% was achieved. In addition, the remaining organic material at final reaction time was analysed by water removal, silylation of the residue and GC-MS analysis of the mixture, but only minor amounts of tartaric, fumaric and oxalic acids could be detected, accompanied with lesser percentages of unknown compounds.

The stability of Fe_{ox} /D3 as catalyst has been evaluated by performing eight consecutive reuses at both pH 4 and 6, monitoring the temporal profiles of the reactions and measuring the iron leaching from the solid catalyst to the solution. Importantly, the Fe_{ox} /D3 catalyst can be easily recovered by filtration, washed with basic water and employed for a new run. Fig. 6 shows that the initial catalytic activity of Fe_{ox} /D3 slightly decreases upon reuse at pH 4, while still achieving complete degradation of phenol. ICP-OES analyses of the solution after catalyst filtration show an iron concentration that decreases from 0.0078 to 0.0065 mg L⁻¹ from the first to the eighth use. These concentrations of iron is much lower than that permitted by European regulations in natural water resources with the value of 0.2 mg L⁻¹ [29]. Furthermore, these values represents a loss of iron from the solid catalyst to the solution between 2 and 1.2 wt.% respect to the initial iron amount of the fresh Fe_{ox} /D3 catalyst. Blank control experiments

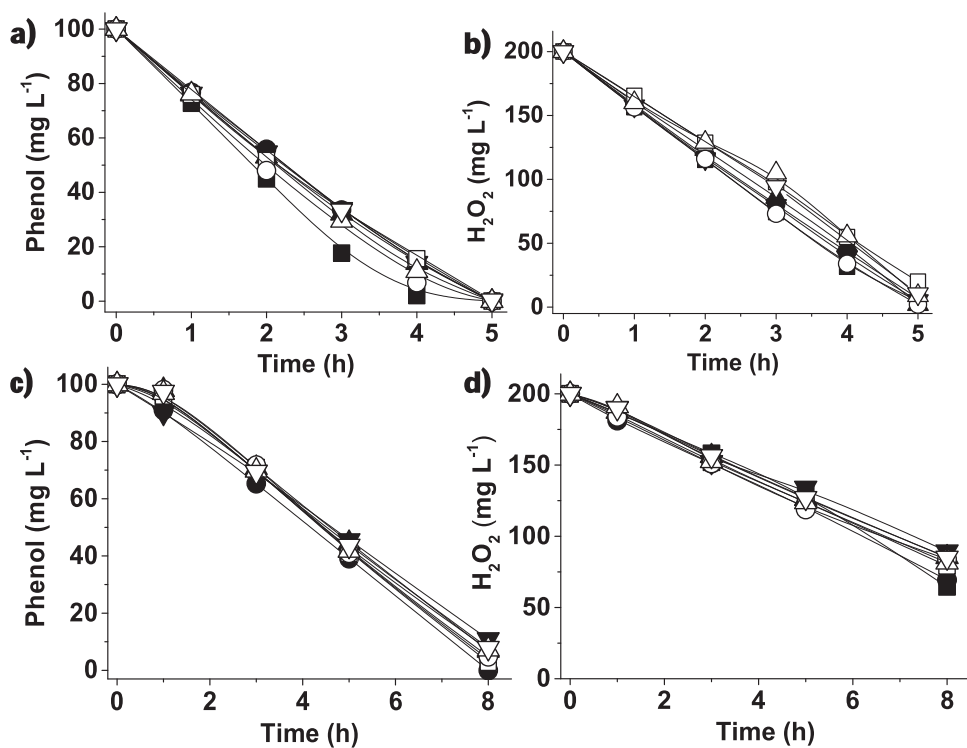


Fig. 6. Catalyst reusability for phenol disappearance (a) and H_2O_2 decomposition (b) at pH 4, and phenol disappearance (c) and H_2O_2 decomposition (d) at pH 6, using $\text{Fe}_{\text{ox}}(0.2 \text{ wt}\%)/\text{D}3$ as heterogeneous Fenton catalyst assisted by visible light irradiation. Legend: (■) First, (●) second, (▲) third use, (▼) forth use, (□) fifth use, (○) sixth use, (△) seventh use and (▽) eighth use. Reaction conditions: catalyst (100 mg L^{-1}), phenol (100 mg L^{-1}), H_2O_2 (200 mg L^{-1}), pH 4, artificial solar light irradiation.

using Fe(II) or Fe(III) salts at the concentration determined for the leached Fe shows much lower activity of the homogeneous reaction than that observed for $\text{Fe}_{\text{ox}}/\text{D}3$ (Fig. S20). Importantly, a productivity test using a large excess of phenol respect to iron by diminishing the amount of $\text{Fe}_{\text{ox}}/\text{D}3$, working at pH 4, allowed estimating an accumulated turnover number (TON) of 38,000 (Fig. S21). One of the most active heterogeneous (photo)Fenton catalysts based on Ag NPs supported on D3 has achieved a TON value under similar conditions of about 472,000 [15]. Considering that iron metal is much more abundant, available and cheap than silver, $\text{Fe}_{\text{ox}}/\text{D}3$ catalyst can be a cost-effective alternative to the use of Ag and noble metals as heterogeneous photocatalyst for the Fenton reaction under visible light irradiation. TEM measurements of the four times used ($3.7 \pm 2.7 \text{ nm}$) and eight times used ($4.6 \pm 3.0 \text{ nm}$) $\text{Fe}_{\text{ox}}/\text{D}3$ catalysts indicate Fe_{ox} NP aggregation respect to the fresh catalyst ($2.2 \pm 0.5 \text{ nm}$) (Fig. 1), but this growth in particle dimension seems not to be reflected on the catalytic activity of the material. It should be noted that the Cu/D3 catalyst deactivates severely upon reuse due to oxidation of reduced copper species Cu(0) and/or Cu(I) to Cu²⁺ and, therefore, reduction by the polyol method was necessary to recover the catalytic activity. Thus, its easier reusability, probably due to the Fenton activity of oxo-hydroxy Fe species with intermediate oxidation states, determines the superiority of $\text{Fe}_{\text{ox}}/\text{D}3$ respect to Cu/D3. Interestingly, $\text{Fe}_{\text{ox}}/\text{D}3$ can be easily reused up to 8 times working at pH values around 6 and observing at this pH value an iron leaching lower than 0.3% respect to the iron supported on D3 (Fig. 6). Notably, at pH 6 iron oxide particle size aggregation was negligible for the four times used ($2.4 \pm 1.8 \text{ nm}$) and eight times used ($2.8 \pm 2.1 \text{ nm}$) $\text{Fe}_{\text{ox}}/\text{D}3$ catalyst compared to the fresh catalyst ($2.2 \pm 0.5 \text{ nm}$) (Fig. S22). This higher catalyst stability of $\text{Fe}_{\text{ox}}/\text{D}3$ at pH 6 compared to pH 4 could be probably due to the higher solubility of Fe species under acid conditions as reflected by the somewhat higher leaching values.

As commented earlier, although the preparation procedure should form initially Fe(0) NPs, they are converted spontaneously into undefined iron oxyhydroxy species. It is also likely that the iron oxyhydroxy species present in the fresh $\text{Fe}_{\text{ox}}/\text{D}$ samples undergo some aging under the reaction conditions due to the action of H_2O_2 . In order to

provide some support to this hypothesis the employed catalysts at both pH 4 and pH 6 were characterized by different spectroscopic techniques. Fig. S23 shows a comparison of FT-IR spectra and diffuse reflectance UV-vis spectra of the fresh and used $\text{Fe}_{\text{ox}}/\text{D}3$ catalyst at pH values of 4 and 6. As it can be seen in this figure, FT-IR spectroscopy shows the appearance of new vibration bands at 622 and 500 cm^{-1} for the used $\text{Fe}_{\text{ox}}/\text{D}3$ catalyst at both pH values 4 and 6. Diffuse reflectance optical spectroscopy of the used catalysts at both pH values also reveals an absorption increase in the region around 420 and 570 nm . It is proposed that these spectroscopic variations are related to the changes in the composition of the Fe oxide. In order to obtain more insights about the possible oxidation of Fe_{ox} NPs supported on D3, characterization of fresh and used unsupported Fe_{ox} NPs treated similarly was also performed (Fig. S24). As expected, also in this case, treatment of Fe_{ox} NPs under the reaction conditions led to changes in the FT-IR, Raman and diffuse reflectance UV-vis spectra, although no changes in the Fe 2p XPS peak were observed, probably due to the overlap between the signals of FeO , Fe_2O_3 or FeOOH as previously reported [30–32]. Therefore, it can be concluded that, both, supported $\text{Fe}_{\text{ox}}/\text{D}3$ and unsupported Fe_{ox} NPs suffers changes in the oxide composition under the reaction conditions in the presence of H_2O_2 at pH 4 and 6.

3.3. Reaction mechanism

The most classical reaction mechanism of photocatalytic reactions of semiconducting metal oxides involves charge separation as the major chemical event following light absorption [33]. To provide some insights about the mechanism of action of $\text{Fe}_{\text{ox}}/\text{D}3$ as photocatalyst a transient absorption spectroscopy study was conducted using an acetonitrile suspension of $\text{Fe}_{\text{ox}}/\text{D}3$ NPs upon excitation with a 532 nm laser. This visible wavelength should induce photoresponse in this sample due to the visible absorption of the iron oxide NPs present on the sample. Upon excitation of the $\text{Fe}_{\text{ox}}/\text{D}3$ suspension, the detection of a transient absorption spectrum decaying in the microsecond timescale characterized by a continuous absorption spanning the whole wavelength range was observed (Fig. 7). The transient absorption spectrum of an acetonitrile suspension of D3 as a blank control has also been recorded,

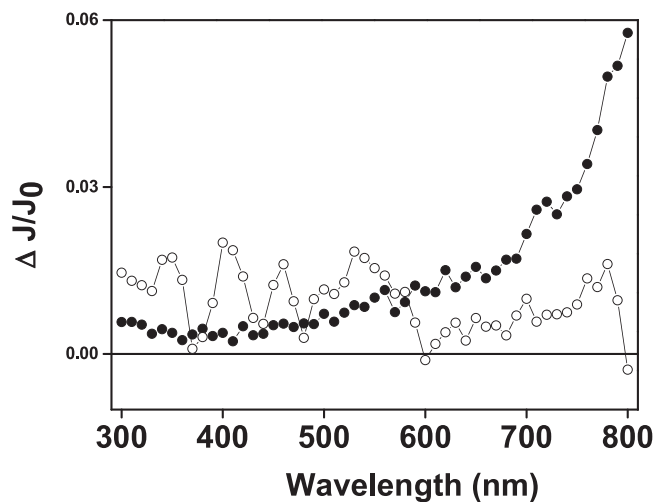


Fig. 7. Transient absorption spectra of an acetonitrile suspension (5 mg ml^{-1}) of unsupported Fe_2O_3 NPs (●) and $\text{Fe}_{\text{ox}}(0.2 \text{ wt}\%)$ /D3 NPs (○) recorded $90 \mu\text{s}$ after 532 nm laser excitation under argon atmosphere.

under the same conditions, observing in this case a negligible transient signal in accordance with the lack of light absorption at 532 nm for this material.

To assign the transient signal recorded for $\text{Fe}_{\text{ox}}/\text{D3}$, the transient absorption spectrum of an acetonitrile suspension of unsupported Fe_2O_3 NPs, synthesized employing the same experimental procedure followed to obtain $\text{Fe}_{\text{ox}}/\text{D3}$, was also recorded under the same conditions. A continuous absorption spanning the whole wavelength range growing in intensity towards the red part of the spectrum was recorded upon excitation of unsupported Fe_2O_3 NPs (Fig. 7). In both cases, the temporal profile of the signals monitored at different wavelengths (400 and 500 nm) are almost coincident (Fig. 8) suggesting that there is only a single transient species absorbing in this wavelength range. We attribute this transient absorption spectrum to the absorption of photo-generated charge separated state with electrons and holes located in different traps in Fe_2O_3 NPs or deposited on D3 in the case of $\text{Fe}_{\text{ox}}/\text{D3}$ [34,35]. In the case of Fe_2O_3 NPs in the absence of D support, a very intense absorption band appears at longer wavelengths ($> 750 \text{ nm}$) at long times after the excitation. Based on the literature, this absorption band at long wavelengths can be attributed to the absorption of solvated electrons in water, supporting the formation of photoejected electrons [34].

To confirm the nature of the transient species photogenerated after the laser pulse, quenching experiments employing O_2 and CH_2Cl_2 as

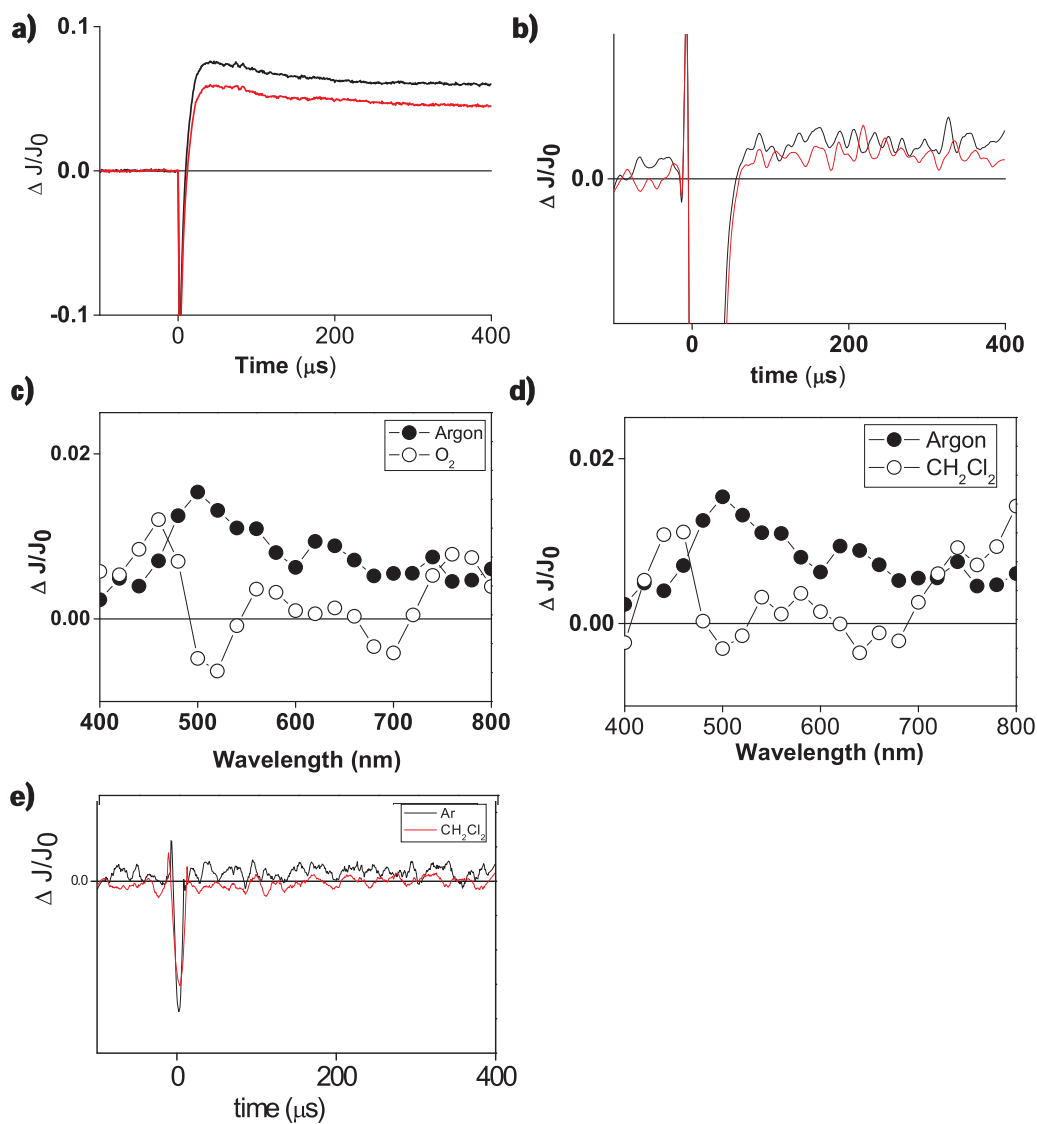
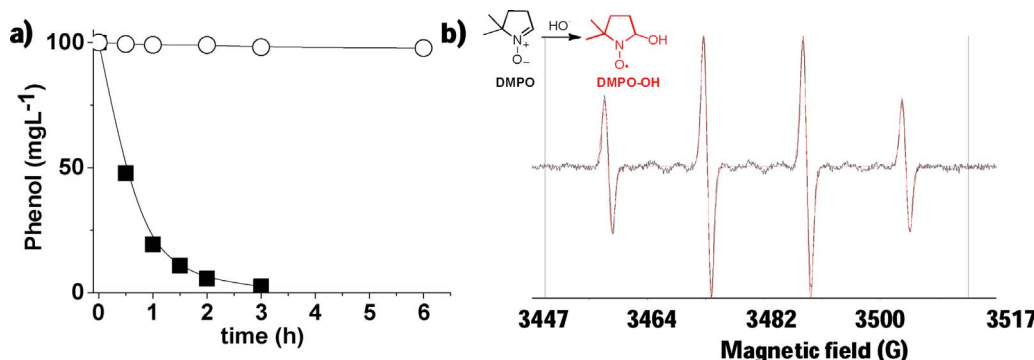


Fig. 8. Temporal profiles of the transient signals monitored at 400 (black line) and 500 (red line) nm recorded after 532 nm laser excitation under argon atmosphere for unsupported Fe_2O_3 NPs (a) and $\text{Fe}_{\text{ox}}(0.2 \text{ wt}\%)$ /D3 (b) suspended in acetonitrile (5 mg ml^{-1}). c) UV-vis transient absorption spectra of an acetonitrile suspension of pure $\text{Fe}_{\text{ox}}(0.2 \text{ wt}\%)$ /D3 NPs recorded $90 \mu\text{s}$ after 532 nm laser excitation: under argon (●), O_2 (○). d) same plot as c) recorded under argon (●) atmosphere or in the presence of CH_2Cl_2 (○). e) Temporal profiles of the transient signals monitored at 500 nm recorded after 532 nm laser excitation under argon atmosphere (black line) and in the presence of CH_2Cl_2 (red line) as electron scavenger for an acetonitrile suspension (5 mg ml^{-1}) of $\text{Fe}_{\text{ox}}(0.2 \text{ wt}\%)$ /D3 NPs. (For interpretation of the references to colour in this figure legend, the reader is referred to the web version of this article.)



referred to the web version of this article.)

electron acceptors were performed [35,36]. Fig. 8c and d show that the transient absorption spectrum recorded upon 532 nm laser excitation of an acetonitrile suspension (5 mg ml⁻¹) of Fe_{ox}/D3 NPs is quenched in the 500 till 700 nm region when any of the two electron quenchers O₂ and CH₂Cl₂ was present. Therefore, the absorption band from 500 to 700 nm of the transient absorption spectrum recorded in the micro-second time scale can be attributed to photogenerated electrons accessible to the quenchers on the external Fe_{ox}/D3 NPs surface.

Besides transient studies, kinetic experiments using quenchers were also carried out to determine the possible nature of the ROS involved in the photoassisted Fenton reaction promoted by Fe_{ox}/D3. Thus, it was observed that the presence of DMSO as selective hydroxyl radical scavenger completely stops the photocatalytic reaction (Fig. 9a). However, the presence of *p*-benzoquinone as selective hydroperoxy radical scavenger has negligible influence on the photocatalytic reaction (data not shown) [13], indicating that HO· radicals are the major ROS involved in the Fe_{ox}/D3 catalyzed photoFenton reaction.

EPR technique was employed to confirm by trapping the main ROS generated during the heterogeneous photocatalytic reaction using Fe_{ox}/D3. Fig. 9b shows the excellent match between the theoretical EPR spectrum for the adduct DMPO-OH· employing the hyperfine coupling constants reported in the literature compared with the experimental one [37]. Detection of DMPO-OH· adduct together with the influence of DMSO in the reaction and the lack of influence of *p*-benzoquinone confirm that the main ROS generated in the photocatalytic reaction using H₂O₂ as oxidant and Fe_{ox}/D3 as catalyst and responsible for phenol degradation is the hydroxyl radical.

Thus, it is proposed that irradiation of Fe_{ox} generates electrons and holes. Electrons will be captured by ambient oxygen or H₂O₂ forming ROS, preferentially HO· radicals, that will trigger phenol degradation. Photogenerated holes will be consumed by the electron donors present in the reaction media, i.e., H₂O₂, phenol and H₂O. Capture of holes by H₂O₂ is proved by a control experiment in which generation of O₂ (the product of hole quenching by H₂O₂) was determined. The amount of O₂ generated in the process decreases by 66% when phenol at the concentration used in the study is present, indicating that this aromatic compound is also competing for hole quenching. Furthermore, H₂O₂ decomposition rate is accelerated by the presence of phenol, indicating that photogenerated e⁻/h⁺ are consumed faster when phenol is present, confirming the role of phenol as hole quencher. The role of diamond should be to act as support facilitating a high dispersion of small Fe_{ox} NPs and an inert surface to release HO· diffusing into the aqueous phase as a free radical [16]. It is known that most of the metal oxide surfaces bind HO· that remains associated to the particles [38] and in this regard the behavior of diamond nanoparticles is very important [15,16].

4. Conclusions

Iron oxide NPs supported on Fenton-treated commercial diamond

Fig. 9. (a) Phenol degradation (a) using Fe_{ox}(0.2 wt%)/D3 at pH 4 in the presence of DMSO as additive (○) and in the absence of DMSO (■). (b) EPR spectrum of the real signal (black line) and the simulated spectrum (red line) of the DMPO-OH adduct (hyperfine coupling constant A_H/G = A_N/G = 14.80). a) Reaction conditions: 100 mg/L phenol, 200 mg/L H₂O₂, suitable pH, 5 mg Fe_{ox}(0.2 wt%)/D3, in the presence or absence of DMSO (1 mL); b) catalyst (100 mg L⁻¹), DMPO (1000 mg L⁻¹), H₂O₂ to DMPO molar ratio 1, pH 4, simulated solar light irradiation, reaction time (5 min). (For interpretation of the references to colour in this figure legend, the reader is referred to the web version of this article.)

NPs followed by hydrogen annealing (Fe_{ox}/D3) at high temperature is a cost-effective catalyst for the heterogeneous Fenton reaction assisted by visible light. Fe_{ox}/D3 exhibits superior catalytic activity than other analogous catalysts based on carbonaceous materials such as AC or G and as well as that of the benchmark photocatalyst Fe_{ox}/TiO₂. Although the activity of Fe_{ox}/D3 is much lower than that of Ag/D3, Fe_{ox}/D3 is active even at quasi-neutral pH values. The heterogeneous photo-Fenton process using Fe_{ox}/D3 can be complemented with a subsequent aerobic biological treatment achieving a biodegradable effluent with tolerable ecotoxicity using only 4 equivalents of H₂O₂ respect to the initial phenol concentration. The most prominent features of Fe_{ox}/D3 respect to other analogous transition metal NPs supported on D NPs previously reported are the easy reusability without the need of reactivation steps and the high activity for phenol degradation and H₂O₂ decomposition under visible light irradiation achieving accumulated TON value of about 38,000. Overall, the present results confirm the suitability of diamond surface as support of active sites to generate free hydroxyl radicals, not attached to the solid surface, that can diffuse into the aqueous phase being highly efficient in the Fenton degradation of organic pollutants.

Conflict of interest

The authors have no competing interests to declare.

Acknowledgements

Financial support by the Spanish Ministry of Economy and Competitiveness (Severo Ochoa and CTQ2015-69153 and CTQ2014-53292-R) and Generalitat Valenciana (Prometeo 2013/14) and is grateful acknowledged. SN thanks financial support by the Fundación Ramón Areces for funding (XVIII Concurso Nacional para la Adjudicación de Ayudas a la Investigación en Ciencias de la Vida y de la Materia, 2016).

Appendix A. Supplementary data

Supplementary data associated with this article can be found, in the online version, at <https://doi.org/10.1016/j.apcatb.2017.12.060>.

References

- [1] J.J. Pignatello, E. Oliveros, A. MacKay, Advanced oxidation processes for organic contaminant destruction based on the fenton reaction and related chemistry, *Crit. Rev. Environ. Sci. Technol.* 36 (2006) 1–84.
- [2] M. Pera-Titus, V. García-Molina, M.A. Baños, J. Giménez, S. Esplugas, Degradation of chlorophenols by means of advanced oxidation processes: a general review, *Appl. Catal. B: Environ.* 47 (2004) 219–256.
- [3] S.R. Pouran, A.R.A. Aziz, V.M.A.W. Daud, Review on the main advances in photo-Fenton oxidation system for recalcitrant wastewaters, *J. Ind. Eng. Chem.* 21 (2015) 53–69.
- [4] K. Ayoub, E.D. van Hullebusch, M. Cassir, A. Bermond, Application of advanced

oxidation processes for TNT removal: a review, *J. Hazard. Mater.* 178 (2010) 10–28.

[5] M.N. Chong, B. Jin, C.W.K. Chow, C. Saint, Recent developments in photocatalytic water treatment technology: a review, *Water Res.* 44 (2010) 2997–3027.

[6] S. Malato, P. Fernández-Ibáñez, M.I. Maldonado, J. Blanco, W. Gernjak, Decontamination and disinfection of water by solar photocatalysis: recent overview and trends, *Cat. Today* 147 (2009) 1–59.

[7] E. Neyens, J. Baeyens, A review of classic Fenton's peroxidation as an advanced oxidation technique, *J. Hazard. Mater.* 98 (2003) 33–50.

[8] S. Navalón, R. Martín, M. Alvaro, H. García, Sunlight-assisted fenton reaction catalyzed by gold supported on diamond nanoparticles as pretreatment for biological degradation of aqueous phenol solutions, *ChemSusChem* 4 (2011) 650–657.

[9] A.D. Bokare, W. Choi, Review of iron-free Fenton-like systems for activating H₂O₂ in advanced oxidation processes, *J. Hazard. Mater.* 275 (2014) 121–135.

[10] S. Chiron, A. Fernandez-Alba, A. Rodriguez, E. Garcia-Calvo, Pesticide chemical oxidation: state-of-the-art, *Water Res.* 34 (2000) 366–377.

[11] J. Herney-Ramirez, M.A. Vicente, L.M. Madeira, Heterogeneous photo-Fenton oxidation with pillared clay-based catalysts for wastewater treatment: a review, *Appl. Catal. B: Environ.* 98 (2010) 10–26.

[12] C. Wang, H. Liu, Z. Sun, Heterogeneous photo-Fenton reaction catalyzed by nano-sized iron oxides for water treatment, *Int. J. Photoenergy* (2012) 801694.

[13] A. Dhakshinamoorthy, S. Navalón, M. Alvaro, H. García, Metal nanoparticles as heterogeneous fenton catalyst, *ChemSusChem* 5 (2012) 46–64.

[14] S. Navalón, A. Dhakshinamoorthy, M. Alvaro, H. García, Heterogeneous Fenton catalysts based on activated carbon and related materials, *ChemSusChem* 4 (2011) 1712–1730.

[15] J.C. Espinosa, S. Navalón, M. Álvaro, H. García, Silver nanoparticles supported on diamond nanoparticles as a highly efficient photocatalyst for the Fenton reaction under natural sunlight irradiation, *ChemCatChem* 7 (2015) 2682–2688.

[16] J.C. Espinosa, S. Navalón, M. Álvaro, H. García, Copper nanoparticles supported on diamond nanoparticles as a cost-effective and efficient catalyst for natural sunlight assisted Fenton reaction, *Catal. Sci. Technol.* 6 (2016) 7077–7085.

[17] D. Sempere, S. Navalón, M. Dančková, M. Alvaro, H. García, Influence of pre-treatments on commercial diamond nanoparticles on the photocatalytic activity of supported gold nanoparticles under natural Sunlight irradiation, *Appl. Catal. B: Environ.* 142–143 (2013) 259–267.

[18] A. Dhakshinamoorthy, S. Navalón, D. Sempere, M. Alvaro, H. García, Reduction of alkenes catalyzed by copper nanoparticles supported on diamond nanoparticles, *Chem. Commun.* 49 (2013) 2359–2361.

[19] Standard Methods for the Examination of Water and Wastewater, 20th ed., American Public Health Association, American Water Works Association, Water Pollution Control Federation, Washington DC, USA, 1999.

[20] R.M. Sellers, Spectrophotometric determination of hydrogen peroxide using potassium titanium(IV) oxalate, *Analyst* 105 (1980) 950–954.

[21] T.K. Townsend, E.M. Sabio, N.D. Browning, F.E. Osterloh, Photocatalytic water oxidation with suspended alpha-Fe₂O₃ particles-effects of nanoscaling, *Energy Environ. Sci.* 4 (2011) 4270–4275.

[22] L.F. Greenlee, J.D. Torrey, R.L. Amaro, J.M. Shaw, Kinetics of zero valent iron nanoparticle oxidation in oxygenated water, *Environ. Sci. Technol.* 46 (2012) 12913–12920.

[23] S. Basavaraja, D.S. BalajiMahesh, D. Bedre, D. Raghunandan, P.M. Prithviraj Swamy, A. Venkataraman, Solvothermal synthesis and characterization of acicular α-Fe₂O₃ nanoparticles, *Bull. Mater. Sci.* 34 (2011) 1313–1317.

[24] L. Gianni, J.L. Zweier, A. Levy, C.E. Myers, Characterization of the cycle of iron-mediated electron transfer from adriamycin to molecular oxygen, *J. Biol. Chem.* 11 (1985) 6820–6826.

[25] O. Allahdin, S.C. Dehou, M. Wartel, P. Recourt, M. Trentesaux, J. Mabingui, A. Boughriete, Performance of FeOOH-brick based composite for Fe(II) removal from water in fixed bed column and mechanistic aspects, *Chem. Eng. Res. Des.* 91 (2013) 2732–2742.

[26] H. Babich, D.L. Davis, Phenol: a review of environmental and health risks, *Regul. Toxicol. Pharm.* 133 (1981) 90–109.

[27] J. Virkutyte, R.S. Varma, Green synthesis of metal nanoparticles: biodegradable polymers and enzymes in stabilization and surface functionalization, *Chem. Sci.* 2 (2011) 837–846.

[28] M. Haruta, When gold is not noble: catalysis by nanoparticles, *Chem. Rec.* 3 (2003) 75–87.

[29] Council Directive 98/83/EC of 3 November 1998 on the quality of water intended for human consumption.

[30] M.C. Biesinger, B.P. Payne, A.P. Grosvenor, L.W.M. Lau, A.R. Gerson, R.S.C. Smart, Resolving surface chemical states in XPS analysis of first row transition metals, oxides and hydroxides: Cr, Mn, Fe, Co and Ni, *Appl. Surf. Sci.* 257 (2011) 2717–2730.

[31] D.L.A. de Faria, S.V. Silva, M.T. de Oliveira, Raman microspectroscopy of some iron oxides and oxyhydroxides, *J. Raman Spectrosc.* 28 (1997) 873–878.

[32] D.M. Sherman, Electronic spectra of Fe³⁺ oxides and oxide hydroxides in the near IR to near UV, *Am. Miner.* 70 (1985) 1262–1269.

[33] W. Wu, C. Jiang, V.A.L. Roy, Recent progress in magnetic iron oxide-semiconductor composite nanomaterials as promising photocatalysts, *Nanoscale* 7 (2015) 38–58.

[34] H.G. Baldoví, B. Ferrer, M. Álvaro, H. García, Microsecond transient absorption spectra of suspended semiconducting metal oxide nanoparticles, *J. Phys. Chem. C* 118 (2014) 9275–9282.

[35] B.C. Fitzmorris, J.M. Patete, J. Smith, X. Mascorro, S. Adams, S.S. Wong, J.Z. Zhang, Ultrafast transient absorption studies of hematite nanoparticles: the effect of particle shape on exciton dynamics, *ChemSusChem* 6 (2013) 1907–1914.

[36] M. Alvaro, P. Atienzar, A. Corma, B. Ferrer, H. García, M.T. Navarro, Photochemical generation of electrons and holes in germanium-containing ITQ-17 zeolite, *J. Phys. Chem. B* 109 (2005) 3696–3700.

[37] M.J. Burkitt, R.P. Mason, Direct evidence for in vivo hydroxyl-radical generation in experimental iron overload: an ESR spin-trapping investigation, *Proc. Natl. Acad. Sci. U. S. A.* 88 (1991) 8440–8444.

[38] Y. Nosaka, A. Nosaka, Understanding hydroxyl radical (OH) generation processes in photocatalysis, *ACS Energy Lett.* 1 (2016) 356–359.